Demonstration of Transmission High Energy Electron Microscopy

F.E. Merrill,[1, a)] A. J. Clarke,[2] J. Goett,[1] J.W. Gibbs,[1] C. Hast,[3] S.D. Imhoff,[1] K. Jobe,[3] F.G. Mariam,[1] C.L. Morris,[1] L.P. Neukirch,[1] J. Perry,[1] D. Poulson,[1] R. Simpson,[1] T. Smith,[3] D. Tourret,[4] P.L. Volegov,[1] P.L. Walstrom,[1] C. H. Wilde,[1] and U. Wienands[5]

[1)] *Los Alamos National Laboratory Los Alamos NM 87544 USA*
[2)] *Colorado School of Mines Golden Co 80401 USA*
[3)] *SLAC National Accelerator Laboratory Menlo Park Ca 94025 USA*
[4)] *IMDEA Materials Institute Getafe Madrid 28906 Spain*
[5)] *Argonne National Laboratory Lamont Il 60439 USA*

[a)] *Corresponding author: fmerrill@lanl.gov*

Abstract. Charged particle radiography with 800 MeV protons has been used for decades at LANL and developed around the world to study dynamic material properties. Recently, charged particle radiography has been demonstrated with the use of high-energy electrons. Because of the difference in the mass of the electron compared to the mass of the proton, the radiographic processes are substantially different and well suited to the study of fast dynamic processes in relatively thin systems. This presentation will show the layout required for such measurements, along with data collected from this recent demonstration performed with 14 GeV electrons generated at the SLAC National Accelerator Laboratory. The radiographic performance for flash measurements will be presented, along with the limitations of this measurement technique.

INTRODUCTION

High energy electron radiography is an extension of proton radiography [1], but at electron energies of 14 GeV new interaction processes become important to the collection of transmitted electrons that form images [2]. Electrostatic lenses are traditionally used to focus low energy electrons in electron microscopy, but electrostatic lenses cannot be used to form the electron images at high energy; only magnetic lenses are strong enough to focus the high energy electron beam. Charged particle radiography using protons has been substantially developed [3] and has proven to be an outstanding tool at several facilities around the world [4, 5, 6, 7] to generate high-resolution measurements of dynamic events for materials studies [8, 9, 10]. Linear accelerator driven light sources, such as the Linac Coherent Light Source (LCLS) at the Stanford Linear Accelerator Center (SLAC), generate photons by passing a multi-GeV electron beam through an undulator. With these high energy electron beams readily available, it is natural to investigate the potential of multi-GeV electron radiography for the study of dynamic systems.

ELECTRON RADIOGRAPHY CONFIGURATION AT SLAC

For these demonstration experiments, a lens with magnification of $\sim$11 was formed from four magnetic quadrupoles, providing a $\sim$ 5 mm field of view in a configuration similar to that developed for high energy proton radiography [11]. A schematic layout of this configuration is shown in figure 1, defining the location parameters of the magnets. Values are shown in table I. All electron radiography measurements were conducted at the SLAC National Accelerator Laboratory at the End Station Test Beam (ESTB) [12], where the 14 GeV LCLS beam was delivered at 5 Hz.

Figure 2 shows the calculated electron trajectories through the magnifier system. These trajectories show the point to point focusing of the electrons, as well as the formation of a Fourier plane downstream of the last quadrupole, where the trajectories are radially sorted by the scattering angle introduced at the object location. Contrast was generated in the electron images by introducing a collimator at this location. Electrons that are scattered to large angles were intercepted and removed by the collimator, while electrons that only undergo small scattering pass through the collimator and go on to form the image at the image location. Four independently actuated copper bars were used for the collimation and contrast generation.

Shock Compression of Condensed Matter - 2019
AIP Conf. Proc. 2272, 060025-1–060025-6; https://doi.org/10.1063/12.0000952
Published by AIP Publishing. 978-0-7354-4000-5/$30.00

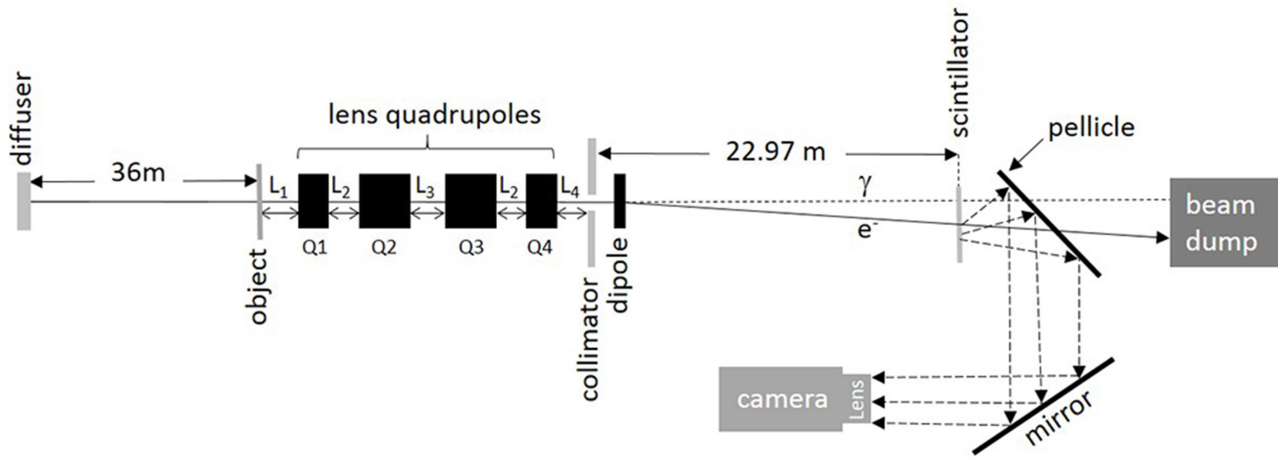

FIGURE 1. Schematic layout of the electron radiography magnifier that was fielded for these measurements.

TABLE I. Parmeters describing the lens configuration shown in figure 1 and the effective length and field gradient of the short (Q1 and Q4) and long (Q2 and Q3) quadrupoles.

Parameter	Value	Parameter	Value
L_1	0.510 m	L^S_{eff}	0.262 m
L_2	0.314 m	G_S	118 T/m
L_3	0.506 m	L^L_{eff}	0.538 m
L_4	0.439 m	G_L	109 T/m

The image collection system was located 23.4 m downstream of the final imaging magnet and was composed of a scintillator, pellicle, and camera. The scintillator was a 400 μm thick columnar cesium iodide scintillator. As electrons traversed the CsI, scintillation light was generated and transported in the $\sim$12 μm diameter crystal columns to the end of the back surface of the CsI screen. The light exiting the back surface of the scintillator was collected by an F1.4 lens and back-thinned CCD camera. The image collected with the CCD camera provided a measure of the flux distribution

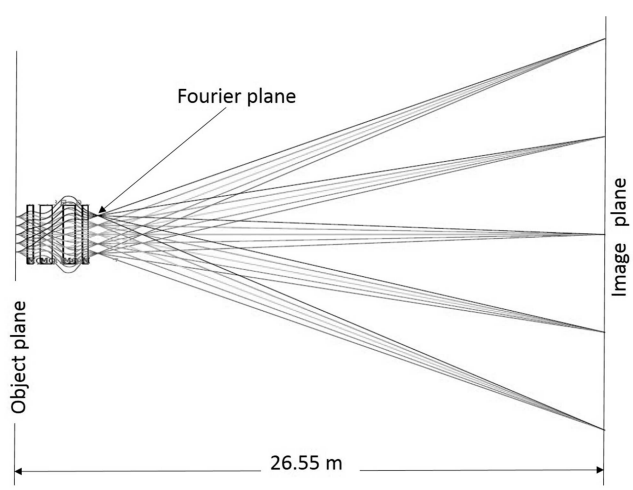

FIGURE 2. Calculated vertical trajectories of the electrons as they pass through the magnifying lens. The lens system generates a Fourier plane downstream of the final quadrupole, where the trajectories are radially sorted by scattering introduced at the object location.

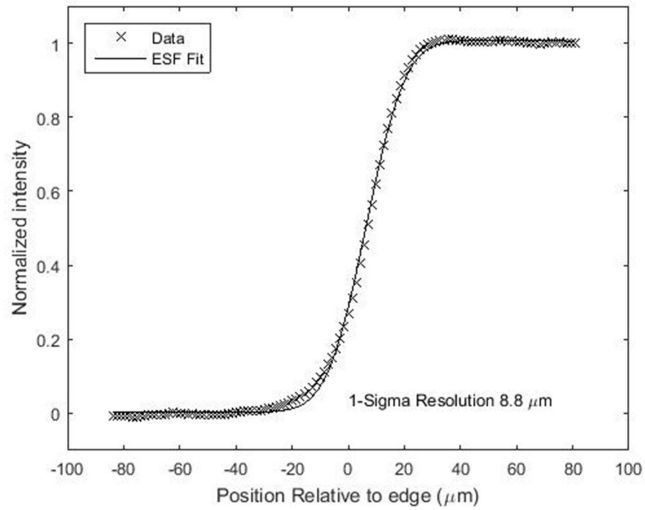

FIGURE 3. Measurement of electron flux across the edge of a tungsten target.

of the focused electrons.

The resolution of this system was measured across a tungsten edge, which is essentially opaque to the electron beam. The spatial extent of the electron flux transition across the edge provides a direct measure of the system edge spread function. An error function fit to this transition region provides an estimate of the resolution, assuming a Gaussian edge spread function. The resolution of the image collection system was measured so it could be removed to estimate the resolution of the microscopy system alone. The resolution of the image collection system was measured from the transition across a black edge placed at the image plane to be 6.7 μm. The radiography resolution is the quadrature difference of the two resolutions. The one-dimensional measure of the edge transition with an error function fit is shown in figure 3. The resolution of the radiography system was determined to be 8.8 μm. This resolution includes any misalignment of the tungsten edge, therefore this resolution is considered an upper limit on the resolution of the radiography system.

Previous studies have shown the resolution of electron radiography degrades with increasing object thickness [13]. Simulations show this resolution degradation is due to large energy tails formed from bremsstrahlung interactions in the object. A small fraction of interactions results in the formation of large energy photons and low energy electrons. These low energy electrons are not properly focused, resulting in resolution degradation. The effect of this process was studied by measuring the resolution of an edge through three thicknesses of tungsten (1 mm, 0.1 mm and no tungsten corresponding to 0.285, .028 and 0 in units of radiation length). Figure 4 shows the edge transition through these three thickness of material. The resolution is not significantly impacted for object thicknesses, which are a small fraction of a radiation length. But when the object thickness becomes comparable to a radiation length, the resolution degrades quickly. This effect limits the technique of high-resolution electron radiography to objects thinner than a radiation length.

ELECTRON RADIOGRAPHY MEASUREMENTS

Induction heaters and chillers were installed at the object location to melt and freeze 200 μm thick samples of metal alloys contained in thin-walled ($\sim$100 μm) boron nitride crucibles, similar to previous experiments [9, 14, 15]. The entire dynamic process, from melting to freezing was monitored over periods of a half hour at $\sim$ 5 Hz. Figure 5 shows a set of eight frames showing the formation of aluminum-rich dendrites in an aluminum-silver alloy during solidification to study micro-structure evolution. The darker contrast corresponds to inter-dendritic regions with increased levels of silver solute. These images highlight the potential of high energy electron radiography for studies of material processing with a large field of view, which is challenging with other imaging techniques.

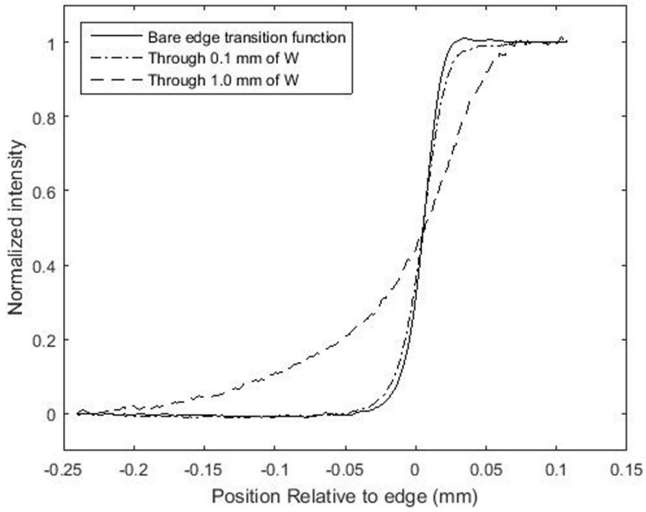

FIGURE 4. Edge transition through three thickness of tungsten (0 , 0.1 and 1 mm of tungsten.) to measure resolution degradation.

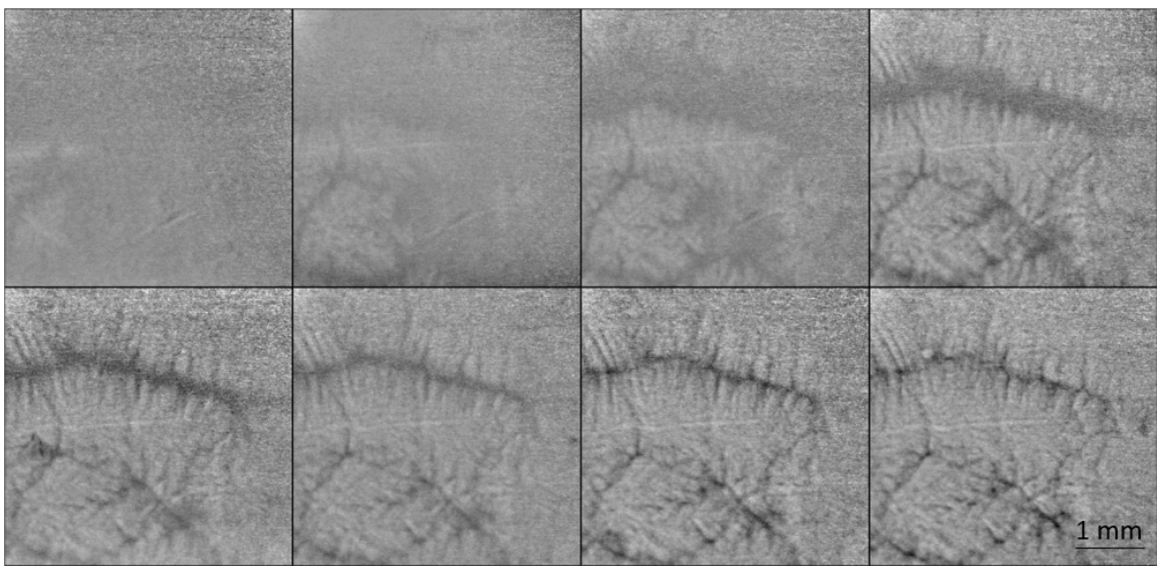

FIGURE 5. Eight transmission frames showing the temporal evolution of an aluminum-silver alloy during freezing. For the first image in the upper left, the sample is in a molten state. Time increase from the left to right and top to bottom.

SYNCHROTON RADIATION

After the electrons pass through the object to be radiographed, the electrons are focused with the magnetic lens system. Electrons passing through these magnets emit synchroton radiation, which could degrade the resolution and perhaps explain the measurement of larger than expected resolution. To understand the effect of this radiation, a series of calculations were performed to estimate the extent of resolution degradation expected from this process.

Electrons passing near the edge of the quadrupole magnet will pass through the largest magnetic field, $B = 1.5T$. The local bending radius, ρ_0 in meters, of electrons in this uniform magnetic field is given by equation 1 [16], with the energy, E in GeV and the magnetic field, B in Tesla

$$\rho_0 = 3.3\frac{E}{B} = 3.3\frac{14GeV}{1.5T} = 30m \tag{1}$$

An electron in this magnetic field will emit synchroton radiation for each orbit and lose energy, dE in MeV, given by equation 2, again with E in GeV and ρ_0 in meters [17].

$$dE = 0.0885\frac{E^4}{\rho_0} = 0.0855\frac{(14GeV)^4}{30m} = 110MeV \tag{2}$$

The length of a magnet is a small fraction of a 30 m orbit, so the total energy lost would be as shown in equation 3, where l is the length of the magnet.

$$dE_m = dE\left(\frac{l}{2\pi\rho_0}\right) = 110MeV\left(\frac{0.262m}{188m}\right) = 0.15MeV \tag{3}$$

If it is assumed that the electron trajectory is located at the highest field in all four lens magnets, the total energy lost would be $\sim$ 450 keV, a fractional energy loss of $3x10^{-5}$. This energy spread, when combined with a chromatic length of $\sim$ 60 m and angular acceptance of $\sim$ 1 mrad results in a blur of 0.2 μm, which is not sufficient to explain the observed resolution degradation.

CONCLUSIONS

Electron radiography, extended to utilize multi-GeV electron beams, is a remarkable diagnostic probe for studying thin systems with high temporal resolution. These first investigations show electron radiography is capable of providing transmission measurements through objects up to a radiation length thick at multiple times having MHz frame rates, with equivalently fast camera systems [18]. With 14 GeV electrons, these radiographs have been demonstrated with better than 10 μm resolution, and theoretical calculations indicate that 1 μm resolution is achievable with a carefully designed and tuned system.

ACKNOWLEDGMENTS

This work was supported by Los Alamos National Laboratory LDRD under DOE/NNSA contract DE-AC52-06NA25396. Solidification experiments were supported by the U.S. DOE, Office of Basic Energy Sciences, Division of Materials Sciences, Award No. DE-SC0016061 and support from Director's Postdoctoral Fellowships from the U.S. DOE through the LANL/LDRD Program. This work performed in part under SLAC DOE Contract DE-AC02-76SF00515

REFERENCES

1. C. L. Morris, N. King, K. Kwiatkowski, F. Mariam, F. Merrill, and A. Saunders, "Charged particle radiography," Reports on Progress in Physics **76**, 046301 (2013).
2. F. Merrill, J. Fabritius, F. Mariam, D. Poulson, R. Simpson, P. Walstrom, and C. Wilde, "Multi-gev electron radiography for measurements of fast dynamic systems," in *AIP Conference Proceedings*, Vol. 1793 (AIP Publishing, 2017) p. 060004.
3. F. E. Merrill, "Flash proton radiography," Reviews of Accelerator Science and Technology **8**, 165–180 (2015).
4. N. King, E. Ables, K. Adams, K. Alrick, J. Amann, S. Balzar, P. Barnes Jr, M. Crow, S. Cushing, J. Eddleman, *et al.*, "An 800-mev proton radiography facility for dynamic experiments," Nuclear Instruments and Methods in Physics Research Section A: Accelerators, Spectrometers, Detectors and Associated Equipment **424**, 84–91 (1999).
5. A. Golubev, V. Demidov, E. Demidova, S. Dudin, A. Kantsyrev, S. Kolesnikov, V. Mintsev, G. Smirnov, V. Turtikov, A. Utkin, *et al.*, "Diagnostics of fast processes by charged particle beams at twac-itep accelerator-accumulator facility," Technical Physics Letters **36**, 177–180 (2010).
6. V. Burtsev, A. Lebedev, A. Mikhailov, V. Ogorodnikov, O. Oreshkov, K. Panov, A. Rudnev, O. Svirskii, M. Syrunin, Y. A. Trutnev, *et al.*, "Use of multiframe proton radiography to investigate fast hydrodynamic processes," Combustion, Explosion, and Shock Waves **47**, 627–638 (2011).
7. D. Varentsov, O. Antonov, A. Bakhmutova, C. Barnes, A. Bogdanov, C. Danly, S. Efimov, M. Endres, A. Fertman, A. Golubev, *et al.*, "Commissioning of the prior proton microscope," Review of Scientific Instruments **87**, 023303 (2016).
8. P. Rigg, C. Schwartz, R. Hixson, G. Hogan, K. Kwiatkowski, F. Mariam, M. Marr-Lyon, F. Merrill, C. Morris, P. Rightly, *et al.*, "Proton radiography and accurate density measurements: a window into shock wave processes," Physical Review B **77**, 220101 (2008).
9. A. Clarke, S. Imhoff, P. Gibbs, J. Cooley, C. Morris, F. Merrill, B. Hollander, F. Mariam, T. Ott, M. Barker, *et al.*, "Proton radiography peers into metal solidification," Scientific reports **3** (2013).

10. L. Smilowitz, B. Henson, J. Romero, B. Asay, C. Schwartz, A. Saunders, F. Merrill, C. Morris, K. Kwiatkowski, G. Hogan, *et al.*, "Direct observation of the phenomenology of a solid thermal explosion using time-resolved proton radiography," Physical review letters **100**, 228301 (2008).
11. F. Merrill, D. Barlow, C. Espinoza, B. Hollander, K. Kwiatkowski, J. Lopez, F. Mariam, D. Morley, C. Morris, P. Nedrow, *et al.*, "Imaging systems for 800 mev proton radiography," Proc. IPAC 2014 , 4057 (2014).
12. M. Pivi, M. Dunning, C. Hast, T. Fieguth, R. Iverson, J. Jaros, K. Jobe, L. Keller, T. Maruyama, D. Walz, *et al.*, "Status of estb: a novel beam test facility at slac," Proceedings of IPAC (2012).
13. F. Merrill, "Imaging with penetrating radiation for the study of small dynamic physical processes," Laser and Particle Beams **33**, 425–431 (2015).
14. A. J. Clarke, D. Tourret, S. D. Imhoff, P. J. Gibbs, K. Fezzaa, J. C. Cooley, W.-K. Lee, A. Deriy, B. M. Patterson, P. A. Papin, *et al.*, "X-ray imaging and controlled solidification of al-cu alloys toward microstructures by design," Advanced Engineering Materials **17**, 454–459 (2015).
15. D. Tourret, J. Mertens, E. Lieberman, S. D. Imhoff, J. W. Gibbs, K. Henderson, K. Fezzaa, A. Deriy, T. Sun, R. Lebensohn, *et al.*, "From solidification processing to microstructure to mechanical properties: A multi-scale x-ray study of an al-cu alloy sample," Metallurgical and Materials Transactions A **48**, 5529–5546 (2017).
16. H. Wiedemann, *Particle accelerator physics* (Springer, 2015).
17. K. Hagiwara, K. Hikasa, K. Nakamura, M. Tanabashi, M. Aguilar-Benitez, C. Amsler, R. Barnett, P. Burchat, C. Carone, C. Caso, *et al.*, "Review of particle physics: Particle data group," Physical Review D-Particles, Fields, Gravitation and Cosmology **66**, 100011–10001958 (2002).
18. K. Kwiatkowski, V. Douence, Y. Bai, P. Nedrow, F. Mariam, F. Merrill, C. L. Morris, and A. Saunders, "Ultra-fast high-resolution hybrid and monolithic cmos imagers in multi-frame radiography," in *Radiation Detectors: Systems and Applications XV*, Vol. 9215 (International Society for Optics and Photonics, 2014) p. 921506.